2-2012

Molecular dynamics simulations of lattice thermal conductivity and spectral phonon mean free path of PbTe: Bulk and nanostructures

Bo Qiu
Birck Nanotechnology Center, Purdue University, qiub3@purdue.edu

Hua Bao
Birck Nanotechnology Center, Purdue University, hbao@purdue.edu

Gengqiang Zhang
Birck Nanotechnology Center, Purdue University

Yue Wu
Birck Nanotechnology Center, Purdue University, yuewu@purdue.edu

Xiulin Ruan
Birck Nanotechnology Center, Purdue University, ruan@purdue.edu

Computational Materials Science 53 (2012) 278–285

Contents lists available at SciVerse ScienceDirect

Computational Materials Science

journal homepage: www.elsevier.com/locate/commatsci

Molecular dynamics simulations of lattice thermal conductivity and spectral phonon mean free path of PbTe: Bulk and nanostructures

Bo Qiu [a,c], Hua Bao [a,c], Gengqiang Zhang [b,c], Yue Wu [b,c], Xiulin Ruan [a,c,*]

[a] School of Mechanical Engineering, Purdue University, West Lafayette, IN 47907-2088, United States
[b] School of Chemical Engineering, Purdue University, West Lafayette, IN 47907-2088, United States
[c] Birck Nanotechnology Center, Purdue University, West Lafayette, IN 47907-2088, United States

ARTICLE INFO

Article history:
Received 2 August 2011
Accepted 15 August 2011
Available online 22 October 2011

Keywords:
Thermal conductivity
Molecular dynamics
Thermoelectrics
Nanostructure

ABSTRACT

In this work, molecular dynamics (MD) simulations are performed to predict the lattice thermal conductivity of PbTe bulk and nanowires. The thermal conductivity of PbTe bulk is first studied in the temperature range 300–800 K. Excellent agreement with experiments is found in the entire temperature range when a small vacancy concentration is taken into consideration. By studying various configurations of vacancies, it is found that the thermal conductivity in PbTe bulk is more sensitive to the concentration rather than the type and distribution of vacancies. Spectral phonon relaxation times and mean free paths in PbTe bulk are obtained using the spectral energy density (SED) approach. It is revealed that the majority of thermal conductivity in PbTe is contributed by acoustic phonon modes with mean free paths below 100 nm. The spectral results at elevated temperatures indicate molecular scale feature sizes (less than 10 nm) are needed to achieve low thermal conductivity for PbTe. Simulations on PbTe nanowires with diameters up to 12 nm show moderate reduction in thermal conductivity as compared to bulk, depending on diameter, surface conditions and temperature.

1. Introduction

High-performance thermoelectric materials have been pursued for several decades. The usefulness of a material for thermoelectric applications is characterized by its dimensionless figure of merit ZT given by $ZT = S^2\sigma T/\kappa$. Here S is the Seebeck coefficient, σ is the electrical conductivity, T is the absolute temperature, and κ is the thermal conductivity containing both electronic and lattice contributions κ_e and κ_l. High-performance thermoelectric materials with high ZT require high S, σ and low κ. PbTe is one of the best thermoelectric materials in the medium temperature range (400–800 K) [1]. Experimentally, Hsu et al. achieved exceptionally high $ZT \sim 2.2$ at 800 K in LAST ($AgPb_mSbTe_{2+m}$) alloys [2]. Harman et al. have observed enhanced ZT in $PbTe/PbSe_xTe_{1-x}$ quantum dot superlattice structures, which has reached the value of 2 at ambient temperature [3]. Androulakis et al. achieved $ZT \sim 1.5$ at 642 K in $(PbTe)_{0.92}(PbS)_{0.08}$ prepared by spinodal decomposition and nucleation and growth approach, with $\kappa_l \sim 0.4$ W/m K [4]. Heremans et al. achieved $ZT \sim 1.5$ at 773 K in $Tl_{0.02}Pb_{0.98}Te$ through distortion of electronic density of states [5]. Roh et al. found reduced thermal conductivity in individual single-crystalline PbTe nanowires grown by a chemical vapor transport method [6]. Fardy et al. studied the thermal conductivity of 180 nm diameter PbTe nanowire and found the thermal conductance to be around 11 nW/K at 300 K [7]. In all these studies, the thermoelectric performance is at least partially due to the low lattice thermal conductivity in PbTe based materials.

Despite the rapid progress in experiments, theoretical understanding of thermal transport in this important material as well as other tellurides lag behind [8–10]. So far, some theoretical investigations have been performed on the electrical transport properties of PbTe and derived materials [11–13]. However, to the authors' best knowledge, very few theoretical works have yet been done to analyze the thermal transport properties of PbTe bulk or nanostructured materials [8,14,15]. Bridging this gap can greatly promote our understanding on heat transfer mechanisms that lead to the relatively low thermal conductivity in PbTe based materials. In addition, with such understanding, we can also examine how various factors (vacancies, dislocations, alloys, nanostructures, etc.) can vary the thermal conductivity of PbTe, aiding the design of better thermoelectric materials with lower lattice thermal conductivity. MD simulation requires no prior knowledge of phonon transport from experiments and can be advantageous in modeling heat transfer across various geometries. Therefore, it's suitable for studying systems at both bulk and nano-scale to provide insight for design of nanostructures.

In this paper, we perform MD simulations to study the lattice thermal conductivity of both PbTe bulk and nanowires. By employ-

* Corresponding author at: School of Mechanical Engineering, Purdue University, West Lafayette, IN 47907-2088, United States. Tel.: +1 7654945721.
E-mail address: ruan@purdue.edu (X. Ruan).

0927-0256/$ - see front matter © 2011 Elsevier B.V. All rights reserved.
doi:10.1016/j.commatsci.2011.08.016

ing the previously developed two-body interatomic potentials for PbTe [14], MD simulations with equilibrium Green–Kubo method are performed to predict the lattice thermal conductivity for both pristine and defected (vacancy) PbTe bulk in the temperature range 300–800 K. Then the lattice thermal conductivity of PbTe bulk with various types and concentrations of vacancies is studied at room temperature. The spectral energy density (SED) analysis is carried out to obtain the spectral relaxation time, mean free path and the contribution of individual phonon branches to the thermal conductivity in PbTe bulk. In the end, PbTe nanowires with diameters from 1.6 to 12 nm are studied for their lattice thermal conductivity dependence on nanowire diameters, surface conditions, and temperature.

2. Molecular dynamics simulations of PbTe bulk

In order to carry out MD simulations, classical interatomic potentials are required. Unlike silicon, germanium, carbon, etc. that have quite a few sophisticated potentials available, classical potentials are not available for most materials, especially for binary or more complicated compounds due to the difficulties in potential developments. So far only two interatomic potentials have been developed for PbTe [8,14] and here we employ the two-body interatomic potentials for PbTe which can reasonably reproduce the mechanical and phonon properties of PbTe bulk crystal [14].

The interatomic potential has the Buckingham potential form

$$V(r_{ij}) = q_i q_j / r_{ij} + A_{ij} \exp\left(-r_{ij}/\rho_{ij}\right) - C_{ij}/r_{ij}^6. \quad (1)$$

Here A_{ij}, ρ_{ij} and C_{ij} are potential parameters, as listed in Table 1. The q_i and q_j are effective atomic charges of the ions which take into account the partial shading of ionic charges by electron clouds. The usage of effective charges rather than formal charges is more appropriate for partially-covalently bonded solids like PbTe when rigid ion model is assumed.

Equilibrium molecular dynamics (EMD) simulation [16] combined with the Green–Kubo linear response formulation [17] is known to be effective in predicting the thermal conductivity of solids. For the cubic systems of interest here, lattice thermal conductivity is given by [18]:

$$\kappa_l = \frac{1}{k_B V T^2} \int_0^\infty \frac{\langle \mathbf{S}(t) \cdot \mathbf{S}(0) \rangle}{3} dt, \quad (2)$$

where V is the volume of simulation domain, T is the temperature, $\langle \mathbf{S}(t) \cdot \mathbf{S}(0) \rangle / 3$ is the heat current autocorrelation function (HCACF) averaged over three directions and $\langle \cdots \rangle$ means the ensemble average. The heat current vector is defined as:

$$\mathbf{S} = \frac{d}{dt} \sum_i \mathbf{r}_i E_i. \quad (3)$$

For a pair potential, the expression can be recast as:

$$\mathbf{S} = \sum_i e_i \mathbf{v}_i + \frac{1}{2} \sum_{i,j} (\mathbf{F}_{ij} \cdot \mathbf{v}_i) \mathbf{r}_{ij}, \quad (4)$$

where $\mathbf{v}_i$ is the velocity of particle i, $\mathbf{F}_{ij}$ is the force between the two particles, and $\mathbf{r}_{ij}$ is the separation. The MD simulation domain is a cubic box consisting of $4 \times 4 \times 4$ unitcells with totally 512 atoms.

Table 1
Parameters of two-body interatomic potential for PbTe employed in this work. Partial charges used to account for electrostatics: Pb: +0.666, Te: −0.666.

	A (eV)	ρ (Å)	C (eV Å^6)	Range (Å)
Pb–Pb	84203.2	0.0754	61.01	16.0
Pb–Te	92131.5	0.2552	585.70	16.0
Te–Te	1773611.7	0.2565	0.61	16.0

At this size, no significant simulation domain size effect is found. The time step is 0.246 fs, which is short enough to resolve all phonon frequencies in PbTe. The system was run for 1,500,000 time steps to extract physical information. Ten independent simulations were run and averaged to minimize the statistical fluctuations. The electrostatic interactions in the system is accounted for by employing the Wolf method, which is shown to reproduce the full Ewald summation with an appropriate choice of parameter α [19]. To carry out MD simulations and calculate the heat current, the system was first run in constant volume and temperature ensemble (NVT) using Nosé–Hoover thermostat [20] to reach thermal equilibrium, then switched to constant volume and energy ensemble (NVE). The heat current was calculated in the last one million time steps, and HCACF was obtained through post-processing of the heat current data. All the simulation results presented here were obtained in this manner and no attempt was made to account for the quantum effects. This is because the temperature range of interest here is higher than the Debye temperature of PbTe, which is 140 K, and the quantum effects are negligible.

Fig. 1 shows the typical HCACF obtained as a function of time. Based on the observed shape of the HCACF, it can be fitted to a sum of two exponential functions:

$$\frac{\langle \mathbf{S}(t) \cdot \mathbf{S}(0) \rangle}{3} = A_1 \exp(-t/\tau_1) + A_2 \exp(-t/\tau_2), \quad (5)$$

as suggested by Mcgaughey and Kaviany [21]. According to Eq. (2), the lattice thermal conductivity can be obtained as:

$$\kappa_l = \frac{1}{k_B V T^2} (A_1 \tau_1 + A_2 \tau_2), \quad (6)$$

The lattice thermal conductivity of PbTe bulk in the temperature range 300–800 K was extracted from MD simulations, as shown in Fig. 2a. The obtained κ_l of pristine PbTe bulk decreases monotonically as temperature increases, which shows clear $1/T$ temperature dependence, indicating the Umklapp phonon–phonon process dominates the phonon scattering. However, as compared to experimental κ_l values [22], the ones from MD simulations are generally larger. Such difference may be due to the presence of defects, impurities, grain boundaries, etc. in experiments, which can lead to lowered thermal conductivity [23].

By realizing that defects or imperfectness can potentially lead to non-negligible alternation to the heat conduction of materials, we study the lattice thermal conductivity of defected PbTe bulk, namely, those with either Pb or Te vacancies. The corresponding MD domains are constructed by removing a designated amount of target atoms (either adjacent to each other or randomly distrib-

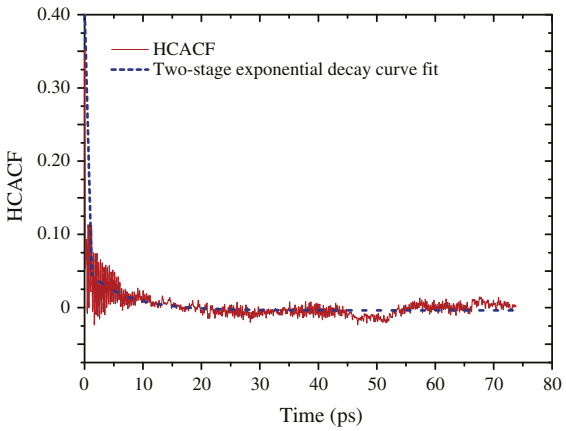

Fig. 1. Typical HCACFs (un-normalized) at temperature 400 K. Dashed curves are the two-stage exponential decay fitting to the HCACFs.

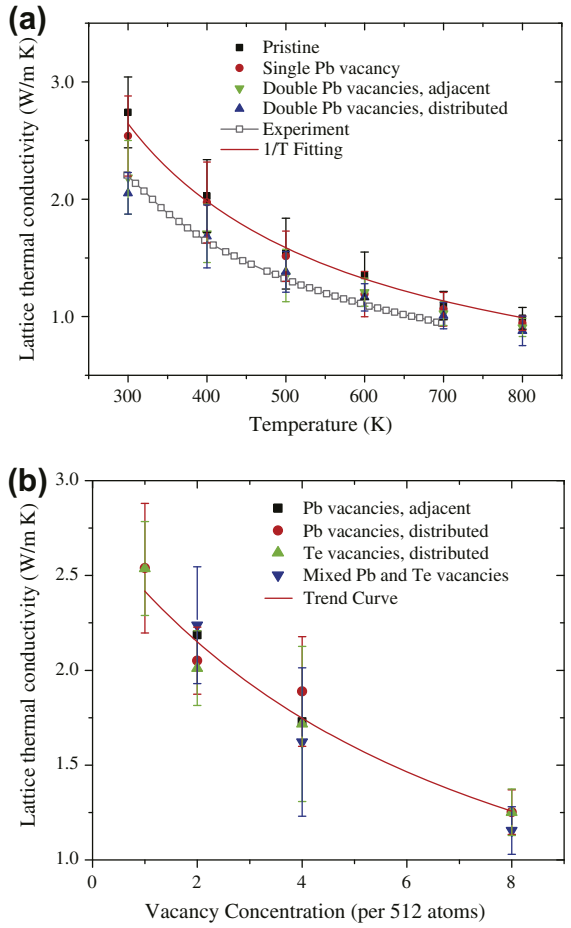

Fig. 2. (a) Predicted temperature dependence of lattice thermal conductivity of pristine and defected PbTe bulk with single and double Pb vacancies, in comparison with experimental values for PbTe bulk [22]. (b) Predicted lattice thermal conductivity as a function of vacancy concentrations for various types of vacancies at room temperature.

uted) from the domain of pristine PbTe bulk with 512 atoms. The obtained temperature dependence of κ_l of PbTe with both single and double Pb vacancies are shown in Fig. 2a, in comparison with MD results of pristine PbTe bulk and experiments. As seen, with single Pb vacancy, κ_l is only reduced by 5% from the pristine one. However, when the vacancy concentration doubles, κ_l is reduced from pristine PbTe by 18% at room temperature, and the values agrees very well with experiments over the entire temperature range under study. This finding is consistent with the fact that natural/unintentional defects are usually present in the fabricated samples [24]. Also it is found that κ_l values of PbTe with adjacent and distributed double Pb vacancies agree with each other over the temperature range. This indicates that κ_l is not sensitive to vacancy spacial distributions, providing that the vacancies are not aggregated to be large enough to form pores in nanometer scale. In addition, it is observed that, as temperature rises, κ_l values of defected PbTe approach those of pristine PbTe, indicating that the contribution of phonon scattering by vacancies to total scattering rate gradually becomes unimportant at higher temperatures, where Umklapp scattering dominates.

On the other hand, room temperature κ_l of PbTe with various types of vacancies as a function of vacancy concentration is plotted in Fig. 2b. As seen, for various types of vacancies studied, as the vacancy concentration increases, the lattice thermal conductivity generally decreases from that of pristine PbTe bulk. Also, it is found that although κ_l values for different types of vacancies vary for a given vacancy concentration, the dependence generally falls onto the same trend described by $\kappa_l \propto 1/(1 + An_v^{-\alpha})$, where n_v is the vacancy concentration and $A = 0.13$, $\alpha = 1.06$ for the presented data. The findings here are consistent with the observations made in diamond and other defects materials [25,26]. Therefore, if there is high vacancy concentration, the lattice thermal conductivity of PbTe may possibly be reduced from that of pristine crystal by as large as 50% at room temperature.

Besides their effects on thermal transport, vacancies might have positive effects on electronic transport properties, for instance, by creating potential barriers to enhance Seebeck coefficient [27]. However, due to the fact that too large defect concentration may significantly deteriorate the transport of electronic carriers, an optimum concentration of vacancies for thermoelectrics may exist and should be verified in future work.

3. Phonon spectral analysis of pbte bulk

To understand the underlying mechanisms which result in the low (more than an order of magnitude smaller than that of silicon) lattice thermal conductivity of PbTe, we examine the vibrational pattern and spectral properties of individual phonon modes through partial phonon density of states (PDOS) and spectral energy density analysis (SED).

As shown in Fig. 3, the PDOS of PbTe are obtained through harmonic lattice dynamics (LD) calculations using the GULP package [28]. It is seen that the vibrational modes of Pb atoms dominate the acoustic regime while those of Te atoms dominate the optical regime. This is largely due to the difference in their atomic mass (Pb: 207; Te: 127.6) that the vibrational frequencies of the heavier Pb atoms are generally lower. Also, it is found that in the acoustic region, the mismatch between the partial phonon DOS of Pb and Te atoms is significant, indicating that correlation between the vibrations of Pb and Te atoms is weak. This suggests that phonon transport across the crystal will suffer from strong scattering, which may be the main reason for the low lattice thermal conductivity in PbTe. These strong scatterings are mainly due to the mass difference and the relatively weak partially covalent bonding between Pb and Te atoms. Similar mismatch in PDOS among constituent elements is also seen in some other low thermal conductivity thermoelectric materials, for instance, Bi_2Te_3 [9,10].

Despite the power of Green–Kubo method in quantitatively studying the lattice thermal conductivity κ_l, only an overall value can be obtained. In many cases, it is also desirable to understand the roles of individual phonon modes in contributing to overall heat conduction. The SED approach does not require any adjustable

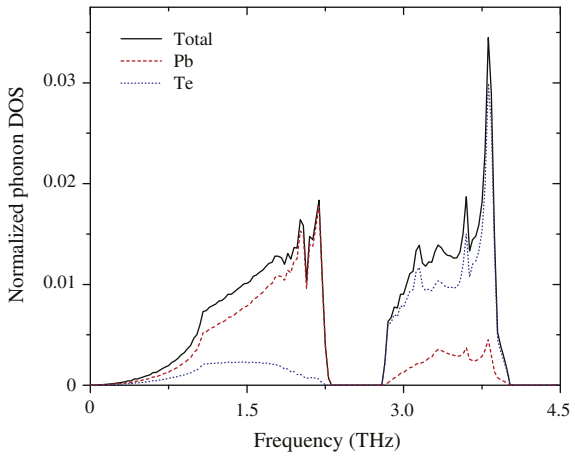

Fig. 3. Normalized partial PDOS for PbTe obtained from LD calculations.

parameters and can be readily integrated with MD simulations to extract the fully-anharmonic phonon frequencies and associated phonon scattering rates for individual modes. Also, it has been well practiced in the past literatures on various materials and proven to be useful in understanding phonon transport in them [29–37]. Therefore, we choose to perform SED on PbTe bulk to quantify the intrinsic phonon scattering mechanisms responsible for its low lattice thermal conductivity.

Starting from the time history of atomic velocities, the SED function can be derived as:

$$\Psi(\mathbf{k},\omega)=\sum_{\alpha}^{3}\sum_{b}^{n_b}\times\frac{m_b}{4\pi\tau_0 N_T}\left|\int_0^{\tau_0}\sum_{l}^{N_T}\dot{u}_{\alpha}^{b,l}(t)\times\exp\left[i\mathbf{k}\cdot\mathbf{r}_0^l-i\omega t\right]dt\right|^2 \quad (7)$$

where $\mathbf{k}$ is the wave vector, ω is the angular frequency, τ_0 is the integration time constant, α represents x, y, z directions, b is the index of basis atoms, n_b is the number of basis atoms in the chosen cell, l is the index of cells, N_T is the total number of cells in the MD domain, and m_b is the atomic mass of basis atom b. Also, $\dot{u}_{\alpha}^{b,l}$ is the α component of the velocity of basis atom b in cell l and $\mathbf{r}_0^l$ is the equilibrium position of cell l. It can be shown [38] that the SED function is a linear superposition of $3n$ Lorentzian functions with centers at the fully-anharmonic phonon frequency $\omega_0(\mathbf{k},\nu)$:

$$\Psi(\mathbf{k},\omega)=\sum_{\nu}^{3n_b}\frac{C(\mathbf{k},\nu)}{\left[2\tau(\omega-\omega_0(\mathbf{k},\nu))\right]^2+1}, \quad (8)$$

where ν is the index of phonon branches and $C(\mathbf{k},\nu)$ is the combination of coefficients as weighting factors for Lorentzian functions. τ is the fully-anharmonic phonon relaxation time. By constructing the SED function based on Eq. (7) using the atomic velocities from MD simulations and fitting Eq. (8) to it, ω_0 and τ can be extracted for a given $\mathbf{k}$.

It should be emphasized that not all $\mathbf{k}$ vectors are allowed in a specific MD domain due to the periodicity requirements. Only those $\mathbf{k}$ vectors in the first BZ associated with the chosen unitcell (either primitive or conventional regardless of the cell choice for MD simulation) satisfying $e^{-i\mathbf{k}\cdot\mathbf{R}}=1$ can be supported by the MD domain and thus resolved in SED. Here $\mathbf{R}=\sum_{i=1}^{3}n_i\mathbf{A}_i$, where $\mathbf{A}_i$ is the length vector of the MD domain in direction i. Therefore, to obtain spectral results along different symmetry directions, the number of allowed $\mathbf{k}$ vectors will be restricted and a large simulation domain is needed to achieve $\mathbf{k}$ grid with reasonable resolution. As suggested by Henry and Chen [30], we reoriented the simulation cells to align the direction of interest with the longest edge of a rectangular domain. In doing this, domains composed of $16\times4\times4$, $16\times6\times4$, and $8\times6\times3$ cells are constructed for [100], [110], [111] directions, allowing 17, 17, and 13 $\mathbf{k}$ points between Γ and BZ boundary. Again, the cells used for each domain are different according to the reorientation.

We obtained phonon relaxation time $\tau_{\mathbf{k},\nu}$ as functions of phonon frequency at 300 and 600 K, respectively, as shown in Fig. 4. For pristine PbTe bulk, the phonon relaxation time should be purely limited by the phonon–phonon scattering. At a temperature that is much higher than Debye temperature of PbTe, normal process is not important and Umklapp process dominates phonon scattering in PbTe bulk. The Umklapp phonon scattering rate τ^{-1} of a particular phonon mode $(\mathbf{k},\nu)$ is the summation of all possible scattering rates involving this mode and other modes in the system, subjecting to both momentum and energy conservation rules [39]:

$$\begin{aligned}&\mathbf{k}_1+\mathbf{k}_2\rightleftharpoons\mathbf{k}_3+\mathbf{G},\\&\hbar\omega_1+\hbar\omega_2\rightleftharpoons\hbar\omega_3,\end{aligned} \quad (9)$$

where $\mathbf{G}$ is the reciprocal lattice vector.

As seen in Fig. 4a and b, the phonon relaxation times resolved in the chosen domains generally span from sub 10 ps to several hundred picoseconds for acoustic phonons at room temperature. These results are in reasonable agreement with the inelastic neutron scattering experiments [40] in both trend and values. Even the anomaly in LA phonons around $\mathbf{k}=(0,0,0.2)$ along $\Gamma-L$ has been reproduced. The apparent overestimated relaxation time here may be attributed to the fact that only intrinsic phonon–phonon scattering is considered for pristine bulk while other mechanisms in the real sample will also contribute to phonon scattering and thus widen the width of phonon peaks (FWHM). As compared to silicon [30], the acoustic phonon relaxation times are roughly about three times smaller in PbTe in average, indicating the large anharmonicity of atomic interactions in PbTe leads to stronger scattering of phonons. As temperature raises to 600 K, the relaxation times of all phonon modes are shortened roughly following T^{-1} dependence. This can be attributed to higher phonon populations with increasing temperature that lead to stronger Umklapp scattering. Also, the relaxation time is generally shorter for phonon with higher frequencies. This can be understood as Umklapp scattering has higher probability to happen for high-$\mathbf{k}$ and high frequency phonons [41] while near-zone-center phonons with low frequencies are less likely to participate in Umklapp process according to Eq. (9). The relaxation times of acoustic phonons were suggested to follow $f^{-\alpha}$ dependence [42], however, in fact the frequency dependent nature of the relaxation times of both longitudinal (LA) and transverse acoustic branches (TA) in PbTe are found to be complicated and deviate from that of f^{-2} relation, consistent with findings in other systems [30,31]. In cases where a $\tau=Af^{-\alpha}$ form is attainable, we find α ranges from 0.8 to 2.0 for LA and TA phonons along different directions, while in other cases lowest order polynomials are used for extrapolation.

As seen in Fig. 4c and d, the optical phonon relaxation times are found to be around 1–5 ps at room temperature and roughly halved at 600 K, consistent with the values estimated from the inelastic neutron scattering experiments [40]. The discrepancy should be attributed to the inaccuracy of the interatomic potentials in reproducing optical phonon dispersion. In contrast to acoustic phonon modes, the relaxation times of optical phonon branches are much shorter, indicating that they are subject to severe scattering. This is because scattering events involving high frequency optical phonons are more likely to satisfy conservation requirements to happen, leading to largely reduced relaxation time [41]. Due to the narrow frequency range of optical phonon modes, their frequency dependence is not clear. Since the contribution from optical phonons to thermal conductivity is small, an averaged value will be used in later analysis without affecting the validness of the results.

As shown in Fig. 5, MFP's of the acoustic phonon modes resolved by the chosen MD domains span from sub 1 nm to 600 nm at room temperature and are shortened when temperature is raised. It is worth pointing out that an estimation based on kinetic theory $\kappa_L=1/3c_v v\,l$, which completely neglects any frequency dependence of phonon properties, gives an effective phonon MFP about 3 nm. Such value can be ambiguous and confusing when one tries to understand reported reduction in lattice thermal conductivity of PbTe based nanostructures with a scale much larger than 3 nm or multi-scales [2,6]. Instead, the knowledge of full frequency dependence of phonon properties is much more useful [43]. As seen, as phonon frequency increases, MFP's of both LA and TA modes monotonically drop by several orders of magnitude, consistent with those found in other systems [30,44]. For LA and

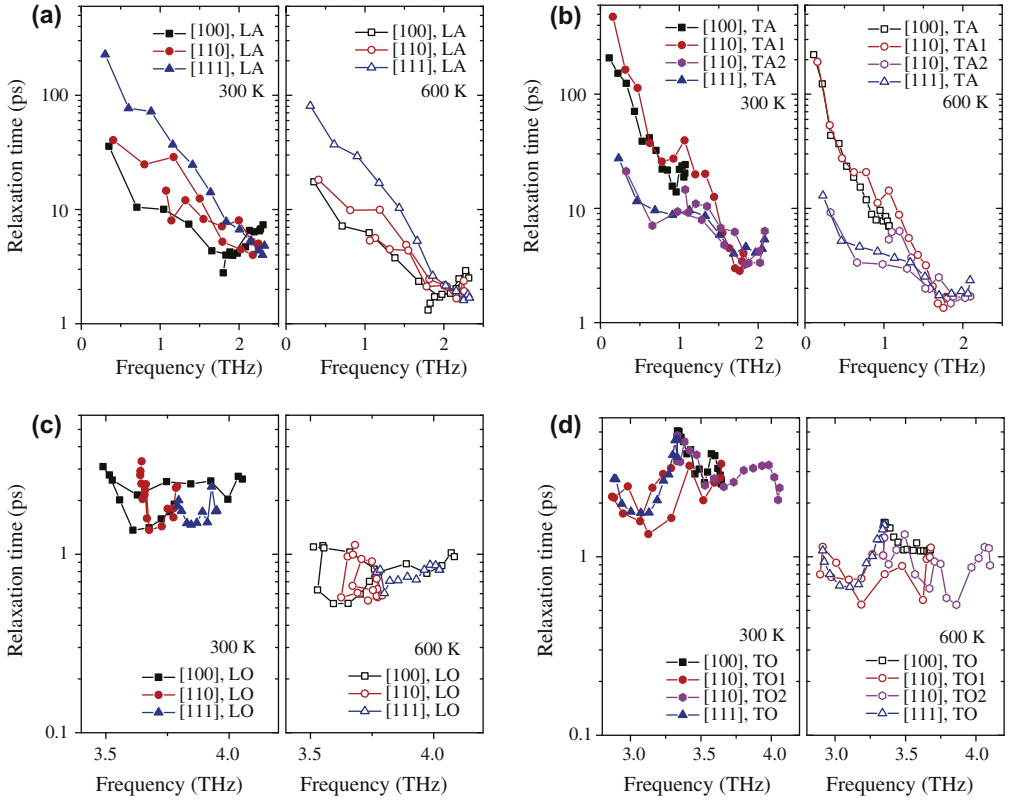

Fig. 4. Phonon relaxation times for (a) LA, (b) TA (1,2), (c) LO, and (d) TO (1,2) branches along [1 0 0], [1 1 0], and [1 1 1] directions as a function of phonon frequency at 300 and 600 K.

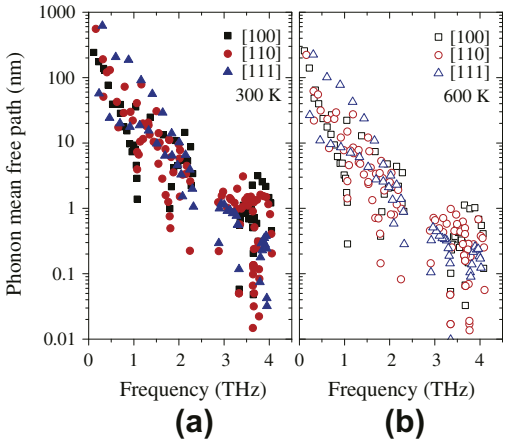

Fig. 5. Phonon MFP as a function of phonon frequency for all phonon branches along [1 0 0], [1 1 0], and [1 1 1] directions in PbTe bulk at (a) 300 K and (b) 600 K.

TA modes in the same frequency range, the MFP's of LA modes are generally larger (not shown), indicating better heat conduction through LA phonon modes in PbTe bulk. In contrast to acoustic phonons, the MFP's of optical phonon modes are generally small. Due to very small MFP and group velocity, the optical phonon modes in PbTe do not carry much heat, and their main influence on heat transfer is made through scattering with acoustic phonons, similar to that in silicon [41].

According to Fourier's law of heat conduction, if isotropic phonon dispersion is assumed, the lattice thermal conductivity can be expressed as:

$$\kappa_l = \frac{4\pi}{3}\frac{1}{(2\pi)^3}\sum_v \int_{\omega_{v,min}}^{\omega_{v,max}} \left(c_v \frac{v_g}{v_p^2}\tau\right)_v \omega^2 d\omega. \quad (10)$$

Here $\omega = 2\pi f$ and the summation goes over all phonon branches. $v_g = d\omega/dk$ is the group velocity and $v_p = \omega/k$ is the phase velocity. The per-mode specific heat c_v is taken as k_B, which is a good approximation at medium temperatures [35]. It should be pointed out that phonon modes in the immediate vicinity of BZ center cannot be easily resolved in SED due to the finite resolution of the **k**-grid and the significant demand of computational resources for a finer **k**-grid. However, the omission of the contribution from these modes is expected to result in underestimation of the thermal conductivity when using Eq. (10). Therefore, the above fitted/extrapolated relaxation times together with the cubic spline fit to phonon dispersion data are used and extended to evaluate Eq. (10) as $f \to 0$. Despite the divergence of acoustic phonon relaxation times near $f = 0$ due to $\tau \sim f^{-\alpha}$, the integral in Eq. (10) is finite and contributions from very low frequency phonons with very long MFP's are not to diverge.

We assume isotropic phonon dispersion then integrate and average over all phonon modes along [1 0 0], [1 1 0] and [1 1 1] directions based on Eq. (10) to obtain the thermal conductivity of PbTe. Such approach has been successfully practiced in literatures [30,32]. Five independent simulations are performed for each case to minimize statistical fluctuations. The obtained lattice thermal conductivity of PbTe bulk is about 3.0 and 1.48 W/m K at 300 and 600 K, respectively, which is within 10% of the value predicted with Green–Kubo method (2.7 and 1.35 W/m K). Such agreement is reasonably well considering the use of isotropic approximation. Despite the small discrepancy, the quantitative understanding of the relative contributions of individual phonon modes to the total lattice thermal conductivity based on isotropic assumption is valid [31,35].

In Fig. 6a, we show the relative contribution to lattice thermal conductivity κ_l from individual phonon branches with respect to

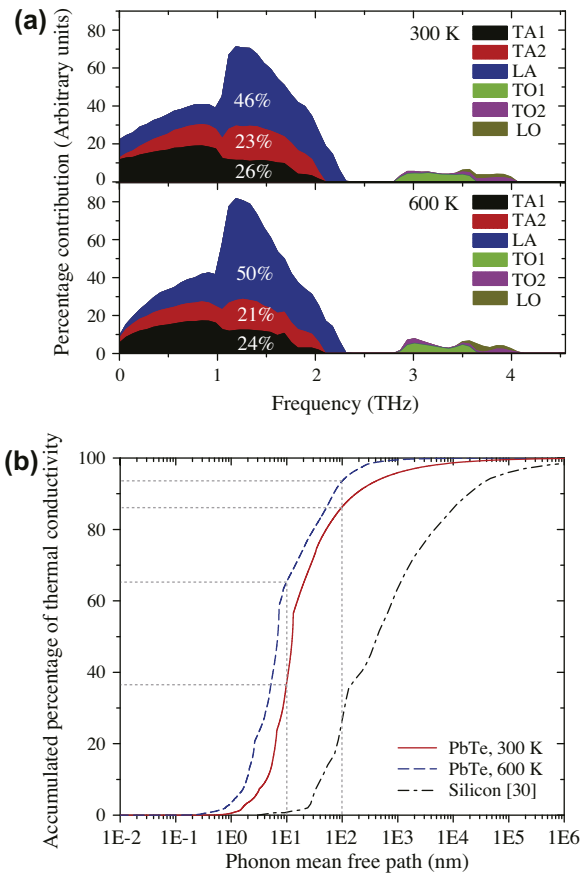

Fig. 6. (a) Percentage contribution to thermal conductivity from individual branches with respect to phonon frequency in PbTe bulk at 300 and 600 K. (b) Accumulated percentage of thermal conductivity with respect to phonon MFP in PbTe bulk at 300 and 600 K, as compared to that of silicon from Ref. [30]. Dotted lines indicate the accumulated percentage from phonons with MFP below 10 and 100 nm, respectively, at 300 and 600 K.

phonon frequency at 300 and 600 K. As seen, the majority of κ_l (95%) is contributed by acoustic phonons at both temperatures. For phonon modes with mid-range frequencies between 1 and 2 THz, due to their large DOS, group velocities and moderate relaxation times, they contribute a significant amount to thermal conductivity. For phonons with frequency below 1 THz, despite their small DOS (Fig. 3), the large relaxation times due to less phonon scattering still allow them to contribute quite a portion to the total thermal conductivity. The two TA branches together contribute about 49% to total κ_l while the LA branch contributes about 46% at room temperature. As temperature increases, the increase of scattering due to U-process in LA phonons appears to be less than that in TA phonons, leading to the 4% increase of LA contributions, mainly from mid-frequency modes. Such observation is consistent with those found in other materials that LA branch contributes the most to thermal conductivity [30,32,35,41]. The remainder of κ_l is contributed by optical phonon branches.

In Fig. 6b, we compare the percentage of accumulation of κ_l with respect to phonon MFP in PbTe at 300 and 600 K together with silicon at 300 K [30]. At room temperature, 86% of κ_l of PbTe is found to be contributed by phonon modes with MFP less than 100 nm. In this portion, more than half of κ_l is contributed by phonons with MFP below 20 nm, in excellent agreement with Koh et al.'s prediction based on Debye-Callaway model [45]. Unlike silicon whose 50% thermal conductivity is contributed by phonons with MFP beyond 1 μm [30,41], only less than 5% of κ_l of PbTe is from phonon modes with very long MFP's, which are mainly near-BZ-center acoustic phonons with wavelengths beyond 25 nm. This is because the major heat carrying phonons in PbTe have MFP's that are at least an order of magnitude shorter than those in silicon. Therefore, nanostructures that are proven to lower the lattice thermal conductivity of silicon may not be efficient in suppressing the thermal conductivity of PbTe. On the other hand, when temperature is raised to 600 K, the MFP's of phonons responsible for the majority of κ_l of PbTe shift downwards roughly by a factor of 2. The consequent temperature effects on thermal conductivity are most prominent when viewing the contribution from phonon modes with MFP below a certain scale. For instance, those phonons with MFP below 100 nm contribute about 93% of κ_l at 600 K, which is only 7% more than that at 300 K. However, phonons with MFP below 10 nm contribute about 65% of κ_l at 600 K while the contribution is halved at 300 K. Therefore, considering the fact that PbTe is mostly used for medium temperature thermoelectrics, in order for PbTe based nanostructures to efficiently suppress lattice thermal conductivity by more than 50 %, nanostructures featuring molecular scales below 10 nm should be pursued.

4. Lattice thermal conductivity of PbTe nanowires

Being inspired by recent experimental and theoretical progress on 1D thermoelectrics [6,7,46,47], we choose to study nanowires to search for possible paths to suppress the lattice thermal conductivity of PbTe. Two types of cylindrical nanowires, i.e., with smooth (SMNW) and sawtooth rough surface (STNW) are studied. Both nanowires are cut from the bulk phase with axial direction along the bulk [100] direction, which is typical for synthesized PbTe nanowires [6]. In light of SED results from the preceding section, SMNWs with diameters from 1.6 to 12 nm are constructed with free boundary conditions applied to surface atoms to allow for reconstruction. The diameter of STNW is defined as that of its core region, so that when comparing its thermal conductivity with that of SMNW, the effects of the core diameter can be ruled out and those of rough surface can be isolated. The diameter of STNWs is varied from 1.6 to 11 nm. The thickness of roughness layer is chosen to be 0.8 nm. In experiments, the roughness observed on nanowire surfaces tends to be disordered and randomized with a certain characteristic scale [46,48]. As an approximation to the realistic roughness, here we constructed nanowires with periodic sawtooth-like rough surface with 383 teeth/μm, as used in earlier BTE studies [49]. The sawtooth-like roughness might not be feasible in experiments due to surface reconstructions. However, the scale of the roughness rather than its shape should be the dominant factor in thermal transport [46,49,50–52], thus the sawtooth model is expected to preserve the physics. We also fixed the outermost surface atoms to ensure stability. Various previous works have used the fixed boundary condition to predict thermal conductivity of nanowires [47,53–57], and in the papers that compared the two boundary conditions, it was concluded that the fixed boundary condition does not have a significant effect on the resulting thermal conductivity. Therefore, we believe our predicted data are still comparable to the experimental data on freestanding nanowires.

The lattice thermal conductivity of SMNWs and STNWs as a function of diameter at room temperature are plotted in Fig. 7. For SMNWs, κ_l decreases with decreasing diameter down to 3 nm, but it increases to $\kappa_l \sim 1.85$ W/m K when the diameter further decreases to 1.6 nm. Similar behaviors in very thin wires were also observed by Donadio and Galli in ideally, H-terminated crystalline silicon nanowires with round cross section [33]. The turn over at atomically thin SMNWs might be an artifact since the nanowire diameter becomes so small to be comparable to the atomic spacings. It might also indicate the transition of thermal transport

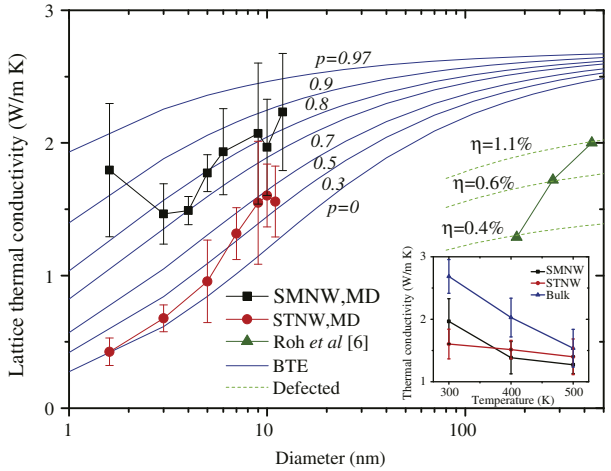

Fig. 7. Lattice thermal conductivity of SMNWs and STNWs as a function of diameter from MD simulations together with BTE results based on Eq. (11) and experimental data from Ref. [6] at room temperature. The inset shows the lattice thermal conductivity of 10 nm diameter SMNW and STNW in comparison with bulk in the temperature range 300–500 K.

from 3D to 1D, as suggested by Donadio and Galli [33]. In contrast, κ_l of STNWs decreases monotonically with decreasing diameter, and is generally at least 25% less than that of SMNWs. When nanowire diameter is larger, the difference in thermal conductivity between SMNW and STNW becomes smaller. This suggests the axial phonon transport experiences less scatterings at the boundaries and has less sensitivity on the conditions of surface roughness in thicker nanowires.

Overall, the thermal conductivity of SMNWs with diameters below 12 nm is reduced by 20–40% compared to bulk. Such reduction is mainly due to the phonon confinement effect on phonon dispersions in 1D nanowires, which leads to reduced group velocities, and thus shorter phonon MFP. Due to the smooth surface of SMNWs, the relaxation time is not expected to degrade much. In fact, despite the strong radial confinement in nanowires, the length of nanowires synthesized experimentally is usually very long (>1 μm), allowing the existence of long wavelength phonons with long MFP's. Therefore, alleviated reduction in κ_l in SMNWs may be found. Similar observation was also made by Donadio and Galli on thin silicon nanowires [33].

On the contrary, more than 50 % reduction is found in STNWs. Part of such reduction likely comes from the fact that the surface roughness layer serves as a second scattering scale in addition to nanowire diameter and efficiently hinders the transport of higher frequency acoustic phonons with wavelengths comparable to the thickness of the roughness layer. On the other hand, for phonons with wavelengths much larger than the radial scale of the nanowire and the thickness of the roughness layers, the particle picture should no longer be valid while a wave description is needed. For these phonons, at the rough nanowire surface layers, phonon waves are likely to experience highly diffusive scatterings, leading to strong phonon interference near the surface region. If we image a traveling wave normally incident on a rigid interface, the interference between the reflected and incident waves will lead to the formation of standing waves adjacent to the interface, with zero time-averaged energy flux. The heat conduction through phonons with long wavelengths and MFP's is largely eliminated in this manner due to the energy localization near thin surface roughness layers. Therefore, with a thin layer of surface roughness, the contributions to κ_l from both the high and low frequency acoustic phonons can be efficiently suppressed. With surface roughness and the 1D phonon confinement in STNWs, considerable reduction in κ_l is thus found.

To better interpret the diameter dependence of the lattice thermal conductivity of nanowires, we solve the Boltzmann transport equation (BTE) for a circular nanowire with appropriate boundary conditions [58] to introduce a diameter-dependent correction factor Q into Eq. (10) as

$$\kappa_l = \frac{1}{(2\pi)^2}\sum_v \int \left(c_v \frac{v_g}{v_p^2}\tau\right)_v Q(p,D)\omega^2 d\omega. \tag{11}$$

Here

$$Q(p,D) = \int_0^{\pi} F(p,D,\theta)\cos^2\theta \sin\theta\, d\theta, \tag{12}$$

where

$$F(p,D,\theta) = 1 - \frac{1-p}{\delta}\frac{1-\exp(-\delta)}{1-p\exp(-\delta)}, \tag{13}$$

and

$$\delta = \frac{D}{v_g \tau \sin\theta}. \tag{14}$$

p is the specularity parameter that reflects the surface scattering conditions, with a value between 0 (diffusive) and 1 (specular). From the phonon spectral results obtained in the previous section, we are able to evaluate the thermal conductivity of nanowires based on Eq. (11), as shown in Fig. 7. As seen, MD data of the thermal conductivity of both nanowires falls well into the envelops of BTE results. The best agreement is achieved when $p \sim 0.8$ and $p \sim 0.4$ for SMNW and STNW, respectively, consistent with the setup that the roughness results in more diffusive scattering at the nanowire surface. The overestimation in atomically thin nanowires from BTE results is because the phonon confinement effects which can alter group velocities are omitted in the solution.

From Fig. 7, it is also seen that, even with fully diffusive surface, a nanowire with pristine crystalline core still sustains thermal conductivity higher than that found experimentally by Roh et al. in 182–436 nm diameter individual PbTe nanowires [6]. To understand such discrepancy, it should be noted that thermal conductivity reduction can also result from possible point defects, dislocation, grain boundaries (in polycrystal nanowires), or non-uniform composition due to varied experimental conditions. Since no measurement data on electrical conductivity or defect concentrations was reported in Ref. [6], it is hard to comment on the quality of the as-grown nanowires. However, in a previous work on PbTe nanowires grown by chemical vapor transport method from the same group [59], they reported the electrical conductivity of these nanowires to be as low as 0.44 S m^{-1}, indicating possible existence of defects that deteriorate the electronic transport. According to Fig. 2b, by scaling BTE results to fit to Roh et al.'s experimental data, the effective vacancy concentrations are found to be between 0.4% and 1.1%, which may reasonably exist under various experimental conditions. As seen, the existing experiments are consistent with our observations and can be interpreted from our MD simulations.

In the inset of Fig. 7, we show the lattice thermal conductivity of 10 nm diameter nanowires in the temperature range 300–500 K. As seen, the temperature dependence of the lattice thermal conductivity of nanowires is generally weaker than that of bulk since the surface scattering is insensitive to temperature. Also, their values are found to be smaller than that of bulk at all temperatures, consistent with the discussions above. However, such reduction is only found to be significant at lower temperatures. To interpret the temperature effects, we realize that MFP of the majority of phonons becomes shorter and comparable to the feature scales of the nanowires as temperature is raised, as seen in Fig. 6b. As a result, the importance of surface scattering in reducing thermal con-

ductivity in nanowires is undermined with the domination of Umklapp process. Therefore, it appears that while nanowire may be a good candidate for room temperature thermoelectrics (e.g., bismuth telluride nanowires [47,48]), its applicability regarding thermal conductivity reduction for high temperature thermoelectric applications may be limited for materials with major phonon MFP around a few tens of nanometers at room temperature (e.g., Bi_2Te_3, PbTe, $CoSb_3$, etc.).

5. Conclusion

In conclusion, MD simulations have been performed to study the lattice thermal conductivity κ_l of PbTe bulk at elevated temperatures and varied vacancy concentrations, as well as PbTe nanowires with different diameters and surface roughness. It is found that κ_l of PbTe bulk decreases with rising temperature and increasing vacancy concentrations. This is due to the phonon Umklapp scattering and vacancy scattering that limit the phonon relaxation time. With about 2% vacancy concentration, κ_l is found to be reduced by up to 50%. It is also observed that κ_l is sensitive to vacancy concentration rather than distribution, providing that the vacancies are not highly aggregated to form nanopores. To understand the low κ_l in PbTe and provide quantitative insight to help the design of PbTe-based nanostructures, we have performed phonon spectral analysis for PbTe bulk. From the partial phonon DOS, we found that the relatively weak correlation between the vibrations of Pb and Te atoms is responsible for the strong scattering in phonon transport across the crystal. We also obtained the spectral phonon relaxation times and MFP's using SED analysis and found the major contribution to κ_l in PbTe is from acoustic phonon modes with MFP below 100 nm. As temperature raises to 600 K, the MFP's of major phonon modes are found to shift downwards roughly by a factor of 2, suggesting feature sizes smaller than 10 nm are needed at higher temperatures to achieve considerable reduction in κ_l of PbTe. From the simulations of PbTe nanowires with diameters up to 12 nm at different temperatures, it is found that with the shrinking of diameter, κ_l is largely reduced by more than 50% for rough and very thin nanowires at room temperature. Such great reduction is attributed to both the strong 1D phonon confinement in thin PbTe nanowires as well as the fact that the surface roughness layers can hinder the transport of both low and high frequency acoustic phonons. It is also seen that the reduction of κ_l in nanowires is alleviated at higher temperatures due to the dominating Umklapp process, which is in consistency with the phonon spectral results.

Acknowledgments

This work was partly supported by a faculty startup fund from Purdue University. B. Qiu also acknowledges the support from the School of Mechanical Engineering, Purdue University. We thank Dr. Alan J. H. McGaughey, Dr. Asegun Henry and Dr. Joseph E. Turney for very helpful discussions.

References

[1] C. Wood, Rep. Prog. Phys. 51 (1988) 459.
[2] K. Hsu, S. Loo, F. Guo, W. Chen, J. Dyck, C. Uher, T. Hogan, E. Polychroniadis, M. Kanatzidis, Science 303 (2004) 818.
[3] T.C. Harman, P.J. Taylor, M.P. Walsh, B.E. LaForge, Science 297 (2002) 2229.
[4] J. Androulakis, C. Lin, H. Kong, C. Uher, C. Wu, T. Hogan, B.A. Cook, T. Caillat, K.M. Paraskevopoulos, M.G. Kanatzidis, J. Am. Chem. Soc 129 (2007) 9780.
[5] J.P. Heremans, V. Jovovic, E.S. Toberer, A. Saramat, K. Kurosaki, A. Charoenphakdee, S. Yamanaka, G.J. Snyder, Science 321 (2008) 554.
[6] J.W. Roh, S.Y. Jang, J. Kang, S. Lee, J.-S. Noh, W. Kim, J. Park, W. Lee, Appl. Phys. Lett. 96 (2010) 103101.
[7] M. Fardy, I.H. A, J. Goldberger, M.M. Zhang, P. Yang, Adv. Mater. 19 (2007) 3047.
[8] T. Chonan, S. Katayama, J. Phys. Soc. Jpn. 75 (2006) 064601.
[9] B.-L. Huang, M. Kaviany, Phys. Rev. B 77 (2008) 125209.
[10] B. Qiu, X. Ruan, Phys. Rev. B 80 (2009) 165203.
[11] S. Ahmad, S.D. Mahanti, Phys. Rev. B 81 (2010) 165203.
[12] Y. Wang, X. Chen, T. Cui, Y. Niu, Y. Wang, M. Wang, Y. Ma, G. Zou, Phys. Rev. B 76 (2007) 155127.
[13] Y. Zhang, X. Ke, C. Chen, J. Yang, P.R.C. Kent, Phys. Rev. B 80 (2009) 024304.
[14] B. Qiu, H. Bao, X. Ruan, ASME 2008 3rd Energy Nanotechnology International Conference, 2008, p. 45.
[15] J. He, S.N. Girard, M.G. Kanatzidis, V.P. Dravid, Adv. Funct. Mater. 20 (2010) 764.
[16] M.P. Allen, D.J. Tildesley, Computer Simulation of Liquids, Clarendon, Oxford, 1987.
[17] R. Kubo, M. Toda, N. Hashitsume, Statistical Physics II, Nonequilibrium Statistical Mechanics, Springer-Verlag, Berlin, 1991.
[18] D.A. McQuarrie, Statistical Mechanics, University Science Books, Sausalito, 2000.
[19] D. Wolf, P. Keblinski, S.R. Phillpot, J. Eggebrecht, J. Chem. Phys. 110 (1999) 8254.
[20] W.G. Hoover, Phys. Rev. A 31 (1985) 1695.
[21] A.J.H. McGaughey, M. Kaviany, Int. J. Heat Mass Transfer 47 (2004) 1799.
[22] V.I. Fedorov, V.I. Machuev, Sov. Phys. Solid State USSR 11 (1969) 1116.
[23] Y. Dong, M.A. McGuire, A.-S. Malik, F.J. DiSalvo, J. Solid State Chem. 182 (2009) 2602.
[24] Y. Gelbstein, Z. Dashevsky, M.P. Dariel, Physica B 363 (2005) 196.
[25] W.D.J. Che, T. Cagin, W.A.G. III, J. Chem. Phys. 113 (2000) 6888.
[26] G.V. Paolini, P.J.D. Lindan, J.H. Harding, J. Chem. Phys. 106 (1997) 9.
[27] K. Kishimoto, M. Tsukamoto, T. Koyanagi, J. Appl. Phys. 92 (2002) 5331.
[28] J.D. Gale, J. Chem. Soc. Faraday Trans. 93 (1997) 629.
[29] A.J.C. Ladd, B. Moran, W.G. Hoover, Phys. Rev. B 34 (1986) 5058.
[30] A. Henry, G. Chen, J. Comput. Theor. Nanosci. 5 (2008) 1.
[31] A.J.H. McGaughey, M. Kaviany, Phys. Rev. B 69 (2004) 094303.
[32] J.V. Goicochea, M. Madrid, C. Amon, J. Heat Trans. 132 (2010) 012401.
[33] D. Donadio, G. Galli, Phys. Rev. Lett. 102 (2009) 195901.
[34] J.A. Thomas, J.E. Turney, R.M. Iutzi, C.H. Amon, A.J.H. McGaughey, Phys. Rev. B 81 (2010) 081411.
[35] J.E. Turney, E.S. Landry, A.J.H. McGaughey, C.H. Amon, Phys. Rev. B 79 (2009) 064301.
[36] N. de. Koker, Phys. Rev. Lett. 103 (2009) 125902.
[37] J. Shiomi, S. Maruyama, Phys. Rev. B 73 (2006) 205420.
[38] J.E. Turney, J.A. Thomas, A.J.H. McGaughey, Predicting phonon properties from molecular dynamics simulations using the spectral energy density, in: Proceedings of ASME/JSME 2011 8th Thermal Engineering Joint Conference (AJTEC2011).
[39] P.G. Klemens, Thermal conductivity and lattice vibrational modes, in: F. Seitz, D. Thurnbull (Eds.), Solid State Physics, Academic Press, New York, 1958.
[40] O. Delaire, J. Ma, K. Marty, A.F. May, M.A. McGuire, M.-H. Du, D.J. Singh, A. Podlesnyak, G. Ehlers, M.D. Lumsden, B.C. Sales, In-plane phonon transport in thin films, arXiv:1103.2564v2.
[41] J.A. Pascual-Gutierrez, J.Y. Murthy, R. Viskanta, J. Appl. Phys. 106 (2009) 063532.
[42] M.G. Holland, Phys. Rev. 132 (1963) 2461.
[43] C. Jeong, S. Datta, M. Lundstrom, J. Appl. Phys. 109 (2011) 073718.
[44] M. Kashiwagi, S. Hirata, K. Harada, Y. Zheng, K. Miyazaki, M. Yahiro, C. Adachi, Appl. Phys. Lett. 98 (2011) 023114.
[45] Y.K. Koh, C.J. Vineis, S.D. Calawa, M.P. Walsh, D.G. Cahill, Appl. Phys. Lett. 94 (2009) 153101.
[46] A.I. Hochbaum, R. Chen, R.D. Delgado, W. Liang, E.C. Garnett, M. Najarian, A. Majumdar, P. Yang, Nature 451 (2008) 163.
[47] B. Qiu, L. Sun, X. Ruan, Phys. Rev. B 83 (2011) 035312.
[48] A. Mavrokefalos, A.L. Moore, M.T. Pettes, L. Shi, W. Wang, X. Li, J. Appl. Phys. 105 (2009) 104318.
[49] A.L. Moore, S.K. Saha, R.S. Prasher, L. Shi, Appl. Phys. Lett. 93 (2008) 083112.
[50] S. Sinha, B. Budhaev, A. Majumdar, Thermal transport in rough silicon nanowires for thermoelectric applications, Mater. Res. Soc. Symp. Proc. 1166.
[51] P. Martin, Z. Aksamija, E. Pop, U. Ravaioli, Nano Lett. 10 (2010) 1120.
[52] P. Martin, Z. Aksamija, E. Pop, U. Ravaioli, Phys. Rev. Lett. 102 (2009) 125503.
[53] J. Carrete, R. Longo, L. Varela, J. Rino, L. Gallego, Phys. Rev. B 80 (2009) 155408.
[54] P. Chantrenne, J.L. Barrat, J. Heat Transfer 126 (2004) 577.
[55] A. Khitun, A. Balandin, K.L. Wang, Superlatt. Microst. 26 (1999) 181.
[56] S.G. Volz, G. Chen, Appl. Phys. Lett. 75 (1999) 2056.
[57] S. Volz, D. Lemonnier, J.B. Saulnier, Nanoscale Microscale Thermophys. Eng. 5 (2001) 191.
[58] J.E. Turney, A.J.H. McGaughey, C.H. Amon, J. Appl. Phys. 107 (2010) 024317.
[59] S.Y. Jang, H.S. Kim, J. Park, M. Jung, J. Kim, S.H. Lee, J.W. Roh, W. Lee, Nanotechnology 20 (2009) 415204.